

Application of dissipative particle dynamics to interfacial systems: Parameterization and scaling

Original

Application of dissipative particle dynamics to interfacial systems: Parameterization and scaling / Ferrari, Marco; Boccardo, Gianluca; Marchisio, Daniele L.; Buffo, Antonio. - In: AIP ADVANCES. - ISSN 2158-3226. - ELETTRONICO. - 13:3(2023), p. 035324. [10.1063/5.0139275]

Availability:

This version is available at: 11583/2977309 since: 2023-04-14T12:36:41Z

Publisher:

AIP

Published

DOI:10.1063/5.0139275

Terms of use:

This article is made available under terms and conditions as specified in the corresponding bibliographic description in the repository

Publisher copyright

AIP postprint versione editoriale con licenza CC BY/Version of Record with CC BY license

Copyright 2023 Author(s). This article is distributed under a Creative Commons Attribution (CC BY) License <https://creativecommons.org/licenses/by/4.0/>."

(Article begins on next page)

Application of dissipative particle dynamics to interfacial systems: Parameterization and scaling

Cite as: AIP Advances **13**, 035324 (2023); <https://doi.org/10.1063/5.0139275>

Submitted: 19 December 2022 • Accepted: 23 February 2023 • Published Online: 15 March 2023

 Marco Ferrari,  Gianluca Boccardo,  Daniele L. Marchisio, et al.



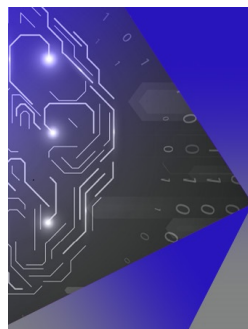
View Online



Export Citation



CrossMark



APL Machine Learning

Machine Learning for Applied Physics
Applied Physics for Machine Learning

**First Articles
Now Online!**

Application of dissipative particle dynamics to interfacial systems: Parameterization and scaling

Cite as: AIP Advances 13, 035324 (2023); doi: 10.1063/5.0139275

Submitted: 19 December 2022 • Accepted: 23 February 2023 •

Published Online: 15 March 2023



View Online



Export Citation



CrossMark

Marco Ferrari,^{a)}  Gianluca Boccardo,  Daniele L. Marchisio,  and Antonio Buffo 

AFFILIATIONS

Department of Applied Science and Technology, Politecnico di Torino, Corso Duca degli Abruzzi 24, 10129 Torino, Italy

^{a)} Author to whom correspondence should be addressed: marco.ferrari@polito.it

ABSTRACT

Dissipative Particle Dynamics (DPD) is a stochastic particle model that is able to simulate larger systems over longer time scales than atomistic modeling approaches by including the concept of coarse-graining. Whether standard DPD can cover the whole mesoscale by changing the level of coarse-graining is still an open issue. A scaling scheme originally developed by Fuchsli *et al.* (2009) was here applied to interfacial systems as one of the most successful uses of the classical DPD method. In particular, equilibrium properties such as the interfacial tension were analyzed at different levels of coarse-graining for planar oil–water interfaces with and without surfactant. A scaling factor for the interfacial tension was found due to the combined effect of the scaling scheme and the coarse-graining parameterization. Although the level of molecular description was largely decreased, promising results showed that it is possible to conserve the interfacial tension trend at increasing surfactant concentrations, remarkably reducing modeling complexity. The same approach was also employed to simulate a droplet configuration. Both planar and droplet conformations were maintained, showing that typical domain formations of multi-component systems can be performed in DPD by means of the scaling procedure. Therefore, we explored the possibility of describing oil–water and oil–water–surfactant systems in standard DPD using a scaling scheme with the aim of highlighting its advantages and limitations.

© 2023 Author(s). All article content, except where otherwise noted, is licensed under a Creative Commons Attribution (CC BY) license (<http://creativecommons.org/licenses/by/4.0/>). <https://doi.org/10.1063/5.0139275>

I. INTRODUCTION

Computer modeling techniques are widely used to enhance the comprehension of the way the molecules organize themselves in a liquid,^{1–3} especially when experimental evidence is hardly available due to the difficulty in isolating individual chemical species.^{4,5} Among molecular techniques, Dissipative Particle Dynamics (DPD) is a well-established method for simulating soft matter systems at the mesoscale level of description.^{6–8} DPD is a coarse-graining technique designed for modeling various fluid systems. For example, this method has been used to simulate particulate suspensions,^{9–11} microfluidic systems,¹² polymer solutions,^{13,14} and interfacial systems.^{5,15–20} Moreover, DPD is well-suited for modeling multi-component systems such as emulsions, and it has been used in a number of studies to look at the effect of adsorbing molecules on the stability of oil or water droplets in emulsions.^{21–24} Therefore, interfacial systems have been largely investigated by

means of DPD due to their remarkable applications to industrial cases, such as food engineering research.⁵ Indeed, DPD has been successfully employed to analyze both static (most notably phase diagrams and interfacial tension calculations)^{5,14,18,25} and dynamic properties (such as transport processes),²⁶ even with amphiphilic and protein molecules acting as surfactants.^{5,15–19}

Initially, DPD was developed to be a truly mesoscopic method, in which both hydrodynamics and thermal fluctuations have a role. In fact, it was considered capable to bridge the whole gap between the atomistic scale, which is accessible by Molecular Dynamics (MD) simulations, and the macroscopic scale, investigated by the continuum modeling approach.⁸ Recent works have seen this ambition of DPD being deeply discussed and developed.²⁷ It was shown that by using a top-bottom approach, i.e., starting from a continuum description and going to the mesoscale, it is possible to obtain a thermo-fluid dynamic consistent method that includes both hydrodynamics and thermal fluctuations at lower scales. This method is

referred to as Smoothed Dissipative Particle Dynamics (SDPD)^{28,29} since it combines Smoothed Particle Hydrodynamics (SPH) and DPD in a way that respects the fluctuation-dissipation theorem through the so-called GENERIC formalism.^{28,29} The main features of this method are the prescription of bead volume and transport properties, which are now input parameters of the simulation, rather than undefined or output values as in classical DPD. Moreover, a lot of effort has been put into addressing many issues of classical DPD, like the resulting unrealistic Equation of State with Many-Body Dissipative Particle Dynamics (MDPD),³⁰ the influence of temperature with Energy-Conserving Dissipative Particle Dynamics (EDPD),³¹ and the lack of all possible friction forces between beads with fluid particle method.³² Speaking instead of the bottom-up approach to mesoscale, the theoretical framework to link the atomistic description and DPD has been recently established through the Mori–Zwanzig projection theory (MZ-DPD), which works very well for bonded atoms–molecules but not so well for unbonded interactions, which are very important in fluid systems to describe transport phenomena like diffusion.²⁷ Mainly for this reason, together with the complexity of the newer DPD methods, classical DPD is still used nowadays by the scientific community, as it is a simpler and computationally cheaper method compared to more rigorous ones, with the caveat that all the parameters must be tuned every time a new system and the corresponding properties of interest are investigated.

In classical DPD, the governing equations are usually expressed in reduced units, which means that the same equations represent a whole family of physical systems.⁸ Fuchslin *et al.*³³ and Arienti *et al.*³⁴ showed that physical properties such as the mass density and the compressibility of a system can be invariant with respect to a specific choice for model parameters that one can associate to the level of coarse-graining. Mai-Duy *et al.*³⁵ applied a similar reasoning also for the viscosity and the Schmidt number.

When applying the appropriate scaling procedure, it was established that a single set of parameters expressed in reduced units represents systems at arbitrary length scales,^{32–34} even for bonded interactions.^{36,37} Such scale independence reported for bulk fluid interactions can hold because the energy associated with an individual particle is made proportional to the number of molecules it represents.³³ On the other hand, surface-dependent interaction parameters may be expected to vary with the level of coarse-graining. In fact, assuming a system that exhibits domain formation, it is physically plausible that those interaction parameters effectively shrink with an increase in the level of coarse-graining. However, if a DPD calculation can be performed at a small scale, then calculations at larger scales will also be feasible, at least with respect to the scaling of parameters.³³

Therefore, in this work, applications of the scaling scheme to oil–water interfacial systems are investigated by means of DPD, also including a coarse-graining procedure for a surfactant molecule referring to our previous work.⁵ Instead of transport processes (viscosity), particular attention is paid to equilibrium properties such as the interfacial tension, highlighting the advantages and limits of the proposed scaling scheme for different levels of coarse-graining. Hence, the combined coarse-graining and scaling procedures are tested for planar interfaces with and without surfactants, and the main findings are eventually compared with the previous work. Finally, an example of simulating a droplet configuration

is also illustrated and discussed. Although many improvements have been made to the original model to include the aspects aforementioned, standard DPD is still recognized as a powerful tool to study interfacial systems. Therefore, the main novelty of this work is to study the effects of upscaling the classical DPD model to different coarse-graining levels while conserving the equilibrium properties of interfacial systems.

This paper is structured as follows: in Sec. II A, general background of the DPD method and of the scaling relations is illustrated; simulation details are provided in Sec. III, together with all assumptions and simplifications of the modeling approach employed; then, the main results are shown and discussed in Sec. IV; and, finally, Sec. V reports the conclusions of this work.

II. THEORETICAL BACKGROUND

An extensive overview of the standard Dissipative Particle Dynamics (DPD) method can be found elsewhere;^{6–8,27,38} therefore, here only the main concepts of this technique are presented, together with the scaling procedure employed in this work.

A. Dissipative particle dynamics

DPD is a stochastic mesoscale particle model that has been devised to allow the simulation of the dynamics of mesoscopic particles, such as colloidal particles and/or groups of molecules, that would require extremely long simulations and very large systems to be studied with atomistic scale molecular modeling technique, such as Molecular Dynamics (MD).^{38,39} Unlike classic MD, each DPD particle i , called a bead, represents a molecular cluster (a molecule fragment or a group of solvent molecules) rather than an individual atom. The DPD system consists of N point particles of mass m_i , position \mathbf{r}_i , and velocity \mathbf{v}_i , whose time evolution is determined by Newton's second law of motion and usually integrated using the modified velocity Verlet algorithm.^{8,40} The major difference between MD and DPD, apart from the coarse-grained nature of the molecules, is the nature of the forces between them. The force \mathbf{f}_i acting on each bead i contains three parts, each of which is pairwise additive,

$$\mathbf{f}_i = \sum_{j \neq i} (\mathbf{F}_{ij}^C + \mathbf{F}_{ij}^D + \mathbf{F}_{ij}^R), \quad (1)$$

where \mathbf{F}_{ij}^C , \mathbf{F}_{ij}^D , and \mathbf{F}_{ij}^R represent the conservative, dissipative, and stochastic (random) forces, respectively, and the sum runs over all other particles within a certain cutoff radius r_c . The dissipative force \mathbf{F}_{ij}^D is a friction term that acts to push particles apart if they are approaching each other and to pull them back together if they are moving apart. It is represented as a pair potential between the particles that conserves both angular and linear momentum. This frictional term leads to a gradual loss of kinetic energy in the system, which is compensated for by the stochastic force \mathbf{F}_{ij}^R to ensure the conservation of energy. The dissipation-fluctuation theorem⁷ leads to a relation between the friction coefficient γ and the DPD-sigma parameter σ , namely the amplitudes of the dissipative and random forces, respectively. These two forces effectively act as a thermostat in DPD, and their mathematical description is investigated in detail elsewhere^{6–8,38} since they are mostly responsible for determining dynamic properties (such as transport processes).^{8,26,41}

Therefore, here only the definition of the conservative force is given since it is involved in studying the static properties of equilibrium systems.^{8,27,41,42} In this work, the conservative force \mathbf{F}_{ij}^C felt by bead i includes contributions from repulsive interactions with surrounding beads and, possibly, contributions due to the springs connecting bead i to other beads in the same molecule. The repulsive force \mathbf{F}_{ij}^r , which is modeled as a soft repulsion between beads i and j , is defined as follows:

$$\mathbf{F}_{ij}^r = \begin{cases} a_{ij}(1 - r_{ij}/r_c)\hat{\mathbf{r}}_{ij} & \text{if } r_{ij} \leq r_c \\ 0 & \text{if } r_{ij} > r_c \end{cases}, \quad (2)$$

where $r_{ij} = |\mathbf{r}_i - \mathbf{r}_j|$ is the distance between beads i and j at positions \mathbf{r}_i and \mathbf{r}_j , respectively, and $\hat{\mathbf{r}}_{ij} = (\mathbf{r}_i - \mathbf{r}_j)/r_{ij}$ is the direction between the two beads. The parameter a_{ij} is the DPD interaction parameter defined for each bead pair, while r_c stands for the cutoff distance. When dealing with a chain molecule, an additional conservative term is considered to maintain bonds between neighbor beads. In this study, the bonds were modeled using a harmonic spring quadratic potential given as

$$U_{ij}^S = k_S(r_{ij} - l_H)^2, \quad (3)$$

where l_H is the equilibrium length for beads i and j , and the stiffness of the length bond constraint is defined by the value of k_S .

B. Scaling relations

In this section, the basic concepts of scaling DPD simulations are presented, along with the nomenclature and notation originally used in the work of Füchslin *et al.*³³

As already stated, the operation of coalescing ν physical particles into one DPD bead is denoted as ‘‘coarse-graining.’’⁴³ Being N the total number of DPD beads in a simulation, it holds that $\nu N = N_{phys}$, with N_{phys} being the number of physical molecules represented in the simulation. In order to compare DPD simulations with different coarse-graining levels ν and ν' , the scaling ratio $\phi = N/N' = \nu'/\nu$ is introduced. Therefore, functions of ϕ are identified to describe the scaling of various quantities at different coarse-graining levels, and these scaling expressions refer to relations between the respective parameters of two systems with different coarse-graining levels ν and ν' . When $\phi > 1$, this means that the same physical space ($L' = L$) is represented by a smaller particle density since each DPD bead in the system denoted by ν' contains a larger number of physical particles. In contrast with the results of Groot and Rabone,⁴⁵ where the bead density ρ is decreased to ρ' while keeping relevant properties (in particular, the particles' radius of interaction) constant, here an alternative scaling process is employed. When changing the level of coarse-graining for the DPD particles, their number is accordingly scaled and their size (radius of interaction) is adjusted in order to keep instead the relative overlap of the interacting particles constant. Hence, when a system with many DPD beads is mapped onto one with fewer but larger and heavier particles, the interaction parameters have to be changed in order to maintain the overall system properties. The following scaling relations in three dimensions are, therefore, here employed:³³

$$\begin{aligned} \nu' &= \phi\nu, & N' &= \phi^{-1}N, \\ m'_i &= \phi m_i, & \rho' &= \phi^{-1}\rho, \\ a'_{ij} &= \phi^{2/3}a_{ij}, & r'_{c,ij} &= \phi^{1/3}r_{c,ij}, \\ \sigma'_{ij} &= \phi^{5/6}\sigma_{ij}, & \gamma'_{ij} &= \phi^{2/3}\gamma_{ij}, \\ \epsilon' &= \phi\epsilon, & \tau' &= \phi^{1/3}\tau, \end{aligned} \quad (4)$$

where $\epsilon = k_b T$ and τ are energy and time scales, respectively, while k_b stands for the Boltzmann constant and T for the temperature. With these scaling relations, the same physical system shares properties, such as mass density, temperature, and compressibility,^{33,35} but it is represented by different coarse-graining levels, using different length and time scales. As it is customary in DPD modeling, energy, mass, time, and length are expressed in reduced units, while parameters in Eq. (4) have to be considered as dimensional quantities.³³ Indeed, the mass of a single DPD particle, force cutoff radius, and thermal energy are typically employed as basic units in DPD. The length, mass, time, and energy of the system are thus not explicitly defined, but rather expressed in terms of these DPD units.⁸ It is also shown that the velocity increments $\Delta\mathbf{v}$ obtained from integrating the forces are unchanged when the scaling is combined with the corresponding reduction of units, which implies that the relative particle motions are unaffected by scaling in the reduced unit systems (denoted by a tilde).³³ Then, when going to the reduced units of the primed system, it gives that for the reduced parameter \tilde{a}_{ij} ,

$$\tilde{a}'_{ij} = a'_{ij} \frac{r'_{c,ij}}{\epsilon'} = \frac{\phi^{2/3}\phi^{1/3}}{\phi} a_{ij} \frac{r_{c,ij}}{\epsilon} = \tilde{a}_{ij}, \quad (5)$$

since a_{ij} scales like energy over length. Similarly, it follows for the reduced $\tilde{\gamma}_{ij}$,

$$\tilde{\gamma}'_{ij} = \gamma'_{ij} \frac{r'^2_{c,ij}}{\epsilon'\tau'} = \frac{\phi^{2/3}\phi^{2/3}}{\phi\phi^{1/3}} \gamma_{ij} \frac{r^2_{c,ij}}{\epsilon\tau} = \tilde{\gamma}_{ij}, \quad (6)$$

since γ_{ij} scales like energy over length and velocity. Finally, from the fluctuation–dissipation relation,⁸ it gives again that

$$\tilde{\sigma}'_{ij} = \tilde{\sigma}_{ij}. \quad (7)$$

These relations indicate that the two coarse-graining systems are stochastically equivalent and, therefore, every system with the same values of the reduced variables \tilde{a}_{ij} , $\tilde{\gamma}_{ij}$, and $\tilde{\sigma}_{ij}$ have the same state space.^{33,35} This implies that, in reduced units, a DPD calculation performed for a system with small extensions and over a small time interval is numerically identical to one performed for a much larger system and covering a longer time range. As a result, it can be shown that DPD is a scale-free (truly mesoscopic) method when dealing with simple bulk fluids.^{33,35} The independence of scale for these systems cannot necessarily be upheld for other types of interactions, namely, binary mixtures of liquids A and B, where more conservative interaction parameters are employed to describe the relative repulsion, such as a_{AA} , a_{AB} , and a_{BB} . Following the scaling relations in Eq. (4), the scale independence holds for bulk interactions (a_{AA} and a_{BB}) because the energy associated with an individual DPD particle scale linearly with ϕ , i.e., it is made proportional to the number of molecules a DPD bead represents.

On the other hand, a_{AB} is a surface-dependent interaction parameter that determines interfacial energy and, therefore, may be expected to scale differently.^{33,34} However, in this work, the original scaling relations in Eq. (4) are used for any pair interaction i, j , and the relative effects will be discussed in Sec. IV, in particular, with regard to the interfacial tension. Therefore, the scaling relations derived by Fuchsli *et al.*³³ are here directly employed for studying their effects on interfacial DPD systems (binary and ternary). Further discussion on their derivation can be found in the original work.³³

When dealing with bonded interactions, the following scaling relations for the parameters k_S and l_H of the harmonic spring quadratic potential [Eq. (3)] are employed:

$$k'_S = \phi^{1/3} k_S, \quad l'_H = \phi^{1/3} l_H, \quad (8)$$

simply obtained by dimensional analysis of units instead of a more sophisticated method.³⁷ Indeed, the stiffness parameter k_s scales like energy over squared length, while l_H scales like length as being the equilibrium length of the bond constraint.

III. SIMULATION DETAILS

In this section, the details of DPD simulations performed are presented, together with the appropriate approximations and simplifications adopted. Two case studies are investigated in this work: first, the interfacial system of a binary mixture modeled via a standard parameterization for the oil and water liquids; and, second, the ternary system where a protein surfactant molecule is introduced and modeled accordingly to our previous work.⁵ For the first case, the effects of applying the scaling relations in Eq. (4) even to a standard interfacial system are studied, and the resulting outcome is used for the second case to scale up the ternary system by comparing the equilibrium properties of the reference model with those of the upscaled one. A last example of a droplet configuration is also provided in order to illustrate the capability of the scaling approach to maintain the domain conformation for multi-component systems.

The simple oil/water interfacial system was simulated in an orthorhombic box of constant size $2L \times L \times L$ with $L = 50$ (in absolute units) with periodic boundary conditions, representing the same physical space for different coarse-graining level ratio ϕ where DPD beads have different radii. This can be seen in Fig. 1 where an example of the simulating boxes of the interfacial oil/water system for $\phi = 1$ (a) and for $\phi = 100$ (b) are reported, highlighting the decrease of the DPD particle number density due to the scaling approach. The initial configuration consisted of a central water phase segregated by two oil phases, thus forming two planar interfaces in equidistant yz -planes. The 50/50 oil-to-water bead ratio was kept constant for all DPD simulations for this case at increasing the coarse-graining ratio ϕ . By denoting the oil bead with O and the water bead with W, typical simulation parameters⁸ in absolute units for $\phi = 1$ are $r_{c,OO} = r_{c,WW} = r_{c,WO} = 1$, $m_O = m_W = 1$, $\rho = 3$, $\gamma_{OO} = \gamma_{WW} = \gamma_{WO} = 4.5$, $\sigma_{OO} = \sigma_{WW} = \sigma_{WO} = 3$, $a_{OO} = a_{WW} = 25$, and a_{WO} ranging from 50 to 100. These parameters have then been scaled according to Eq. (4) for other coarse-graining values of ϕ . Following the energy and time scaling in Eq. (4), DPD simulations were run with a time step $\Delta t = 0.02\tau$ for 10^4 equilibration steps

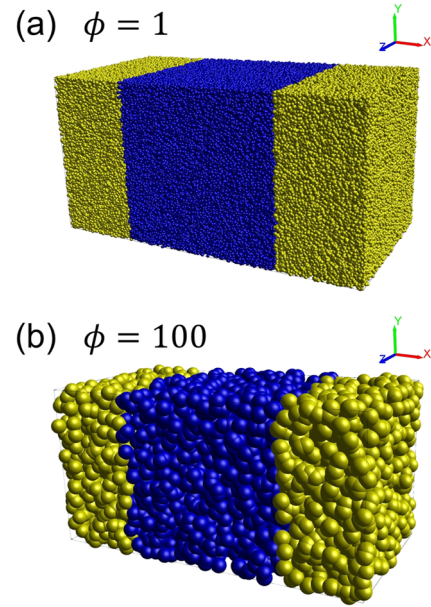


FIG. 1. Snapshots of DPD boxes of the planar interfaces between oil (yellow) and water (blue) for $\phi = 1$ (a) and for $\phi = 100$ (b).

and for a production period of 5×10^4 steps. Pressure and interfacial tension were then measured from simulations. In particular, the interfacial tension (IFT) was computed by integrating the difference between normal and tangential stress across the interface separating the segregated components.⁴⁴ Therefore, if the normal to the interface lies along the x -direction, the interfacial tension (in physical unit) is deduced from the local components of the pressure tensor,

$$\text{IFT} = \frac{1}{2} \int (p_N - p_T) dx = \frac{1}{2} \int \left(p_{xx} - \frac{1}{2}(p_{yy} + p_{zz}) \right) dx, \quad (9)$$

where p_N and p_T are the normal and tangential components of the pressure tensor profile, respectively. The factor 1/2 before the integral sign is due to the presence of two symmetric interfaces in the DPD simulation box when using periodic boundary conditions.

The second case, where the scaling approach was tested, focused on reproducing a ternary system made of water, oil, and protein surfactant, which was investigated in our previous work,⁵ and thus labeled here as the reference model for $\phi = 1$. The general idea is, therefore, to scale the DPD model up to the protein molecule level by maintaining the appropriate differences between the three phases. In the reference model, the protein surfactant was modeled as a chain molecule with bonded interactions. Here, this level of detail will be lost, favoring instead the mutual repulsion with the remaining two phases (oil and water). First of all, the new coarse-graining level v' (and ϕ) was decided in order to represent the protein molecule as a single DPD particle or as two bonded beads. In line with the volume equivalence of DPD particles employed in previous studies,^{5,41,45} the coarse-graining level ratio $\phi = v'/v$ was chosen by referring to the protein molecule size, namely, by comparing the bead volume of the primed system with

that of the reference model. As it has been shown, the protein molecule assumed an almost stable mean radius of gyration of about 36.5 Å after a certain surface concentration at the oil/water interface.⁵ As a first guess when the protein molecule was modeled with a single DPD bead, this value is then assumed as the radius of the sphere whose volume is compared with that used in the reference model for defining the coarse-graining level ν , namely, the volume of a cluster of three water molecules.^{5,45} This leads to preserving bead-size effects when dealing with chain molecules^{37,45} instead of simply comparing the number of beads representing the protein molecule in the reference model. So the coarse-graining ratio ϕ was defined as the ratio of particle volumes: 3008 and 1504 for coarse-graining the protein as a single bead (P) and as two bonded beads (H and T), respectively (Fig. 2). Therefore, the scaling procedure was applied to the ternary system with these values of ϕ , making the comparison with the reference model. Water (W) and oil (O) beads are then represented by taking into account the coarse-graining ratio ϕ , respectively, employed. While the water bead in the primed system is made by coalescing ν' number of physical water molecules, oil was also modeled as a chain molecule in the reference system, thus the ratio between the protein and oil molecular volumes gives the number of oil molecules gathered to represent the O bead in the primed system.

As it was performed for the simple O/W interfacial system, all DPD simulations of the ternary interfacial system were performed in an orthorhombic box of constant size $2L \times L \times L$ with $L = 128$ (in absolute units) with periodic boundary conditions. This box size was employed in order to simulate a total number of particles N' large enough to gather statistically relevant results. For the interfacial system, the 50/50 oil-to-water bead ratio was again kept constant, and both the number of water and oil beads filling the simulation box were adjusted to keep the same overall number density ρ' when the protein beads were also added in the DPD box. Indeed, simulations were performed to study equilibrium properties of the interfacial system, such as the interfacial tension, at increasing protein surfactant concentrations, where its surface number density was calculated as will be explained in the Appendix. The initial configuration again here consisted of a central water phase segregated by two oil phases, thus forming two planar interfaces in equidistant yz -planes. The protein molecule beads were initially located at the oil–water interface to make sure that both interfaces contain the same number

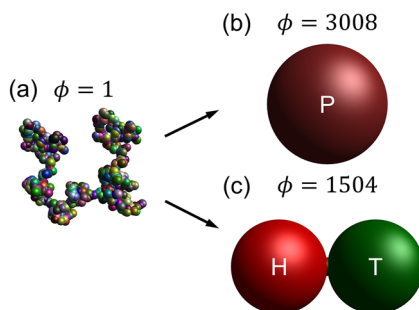


FIG. 2. Schematic representation of the coarse-grained protein molecule in the reference DPD model⁵ with $\phi = 1$ (a) and in the upscaled DPD model with $\phi = 3008$ (b) and $\phi = 1504$ (c).

TABLE I. Repulsion parameters a_{ij} used in this work. Note that these parameters have to be scaled according to Eq. (4) based on the value of $\phi = 3008$.

a_{ij}	W	O	P		
			Case 1	Case 2	Case 3
W	25				
O	16.5	50			
P	Case 1	60	90	30	
	Case 2	70	105		35
	Case 3	80	120		40

of surfactants in order to perform averages on both interfaces. In line with our previous work⁵ for $\phi = 1$, the simulation parameters in absolute units are $\rho = 5$ and $\gamma_{ij} = 4.5$, $\sigma_{ij} = 3$, for any bead pair ij , then scaled according to Eq. (4) for corresponding coarse-graining values of ϕ (3008 or 1504). $m'_p = 2m'_H = 2m'_T$ is determined by the ratio between the molecular mass of the protein and that of three water molecules, while m'_O by the ratio of the oil molecule mass and that of three water molecules multiplied for the number of oil molecules coalesced in the O particle based on the ϕ value used. With regard to the repulsion a_{ij} parameters, they are listed in Tables I and II, and, apart from $r_{c,WO} = 1$, $r_{c,ij}$ is equal to 0.7 according to Ferrari *et al.*⁵ for $\phi = 1$. In addition, these parameters have been scaled following Eq. (4). It is straightforward to underline here that the self-repulsion parameters of oil and water (a_{WW} and a_{OO}) have been obtained by respective bulk simulations. Since the pressure of bulk fluids is independent of the coarse-graining ratio ϕ by means of Eq. (4), a_{WW} was exactly the same as used in the reference work,⁵ while a_{OO} was determined by letting the oil bulk phase pressure in the primed system being the same as for $\phi = 1$ (results not shown). The inter-repulsion parameters were obtained in order to give the best matching with the interfacial tension values, as it will be shown in Sec. IV. In particular, three parameterization cases have been tested for the P bead when the protein molecule was modeled as a single particle, while a clear distinction between the hydrophilic (H) and hydrophobic (T) parts was made if the protein was described by two beads. Therefore, when applying such a coarse-graining procedure, the obtained repulsion parameters were still representative of surfactant interactions, but the level of molecular details was much smaller than in the case of $\phi = 1$. Moreover, the harmonic potential parameters used for the bond between H and T beads are $k_S = 400$ and $l_H = 1$, as a first guess, then scaled according to Eq. (8). Following again the time and energy scaling in Eq. (4), these DPD simulations were performed with a time step $\Delta t = 0.001\tau$ for 3×10^4

TABLE II. Repulsion parameters a_{ij} used in this work. Note that these parameters have to be scaled according to Eq. (4) based on the value of $\phi = 1504$.

a_{ij}	W	O	H	T
W	25			
O	16.5	50		
H	20	200	15	
T	90	40	15	15

equilibration steps and a production period of 10^5 steps. Density profiles, pressure, and interfacial tension were then measured from the simulations. Here the interfacial tension was calculated again as reported in Eq. (9).

An illustrative test was also conducted by simulating an oil droplet in bulk water in the presence of protein surfactants at equilibrium in order to investigate the capability of the parameterization employed and the scaling procedure for an additional interfacial system setup. For both $\phi = 3008$ and $\phi = 1504$, the initial conditions and the physical space simulated are the same. Being $R = 65$, the initial radius of the sphere containing the oil phase, DPD simulations were performed in a cubic box with $L = 4R$. As in the previous case, these box dimensions were used to simulate a number of total particles N' large enough to gather statistically relevant results. The sphere was then filled with oil beads and the remaining space with 700 protein molecules (single bead or two-bead molecule depending on the value of ϕ adopted) and with a number of water particles in order to have an overall $\rho = \phi\rho'$ equal to 5. The same simulation parameters were employed and, in particular, only case 3 of Table I was studied for the P bead type parameterization. Simulations were run for a total of 2.5×10^5 steps, out of which 5×10^4 steps are used to equilibrate the system, saving time frame data for post-processing every 250 steps. Therefore, the time-averaged distributions of the radius of gyration of the oil droplet surrounded by protein molecules were then measured for both ϕ cases.

All DPD simulation setup, runs, and post-processing analyzes were conducted within the CULGI software package,⁴⁶ along with all other tools and algorithms employed in this work.

IV. RESULTS AND DISCUSSION

In this section, the main findings of our work are presented and discussed. First, the analysis of the simple DPD O/W interface is carried out, and then, applications of the scaling procedure to more complex systems are reported.

Figure 3 shows the pressure (a) and IFT' (b) trends with varying the coarse-graining ratio ϕ for the simple O/W interface for three values of the a_{WO} parameter. A relatively small non-linear increment is detected with regard to pressure values at increasing ϕ . Fuchslin *et al.*³³ already reported that pressure in a DPD simulation of a bulk fluid with periodic boundary conditions for different self-repulsion parameters a and for various ϕ values is independent of the coarse-graining. Therefore, applying the scaling relations in Eq. (4) to a binary system leads to the loss of pressure independence of the coarse-graining ratio. This can be related to the use of the same scaling expression for the surface term a_{WO} .³³ Therefore, a limitation of such a scaling scheme is observed since the pressure of the binary mixture might not be conserved with increasing the level of the coarse-graining ratio. On the other hand, for each a_{WO} value, it is clearly evident that the interfacial tension (in physical unit) IFT' computed from DPD simulations [Eq. (9)] scales with ϕ^C , where $C = 1/3 \leq 1$, as suggested by Fuchslin *et al.*³³ so that

$$IFT' = \phi^{1/3} IFT. \tag{10}$$

It is important to highlight here that this result is in line with the works of Arienti *et al.*,³⁴ Vanya, Sharman, and Elliott.⁴⁷ Such a scaling relation for the interfacial tension can be expected from the

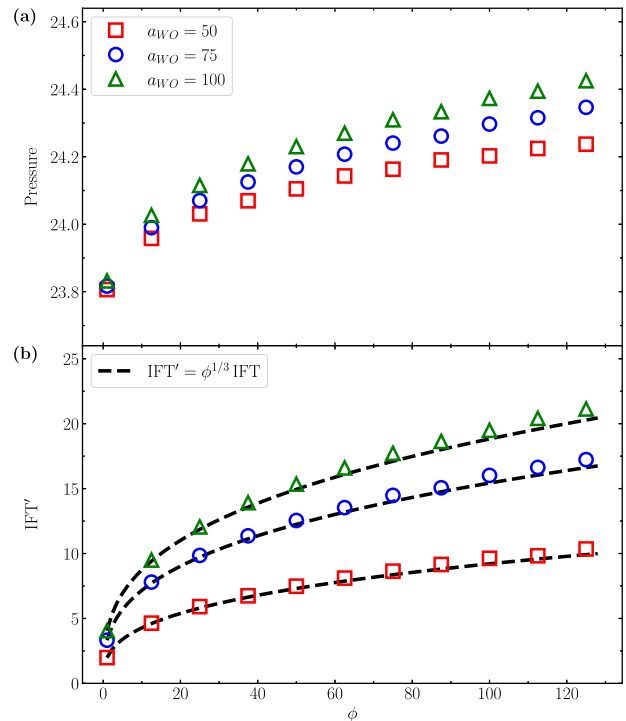


FIG. 3. Pressure (a) and IFT' (b) trends with varying the coarse-graining ratio ϕ for the simple O/W interface. Empty symbols stand for the results of DPD simulations with the repulsion parameter a_{WO} equal to 50 (red squares), 75 (blue circles), and 100 (green triangles), respectively. Black dashed lines represent the scaling relation for the interfacial tension: $IFT' = \phi^{1/3} IFT$.

dimensional analysis of units in Eq. (4). In fact, following the notation of the reduction of units from the work of Fuchslin *et al.*,³³ it is also possible to show that

$$\widetilde{IFT}' = IFT' \frac{r_c'^2}{\epsilon} = \phi^{1/3} IFT \frac{\phi^{2/3} r_c^2}{\phi \epsilon} = \widetilde{IFT}, \tag{11}$$

since interfacial tension reduces as energy over squared length. Hence, scaling and unit reduction precisely cancel each other. As a result, in the DPD framework, the reduced interfacial tension \widetilde{IFT} is scale-free, meaning that the calculation of this equilibrium property with a single set of parameter values represents interfaces at arbitrary length scales. In order to study how the scaling relations affect the interfacial tension calculation, the stress profiles of the simple O/W system along the normalized x -direction normal to the interfaces at increasing coarse-graining ratios ϕ are shown in Fig. 4. The mechanical equilibrium of the system is reached in both the oil and water phases since the stress profiles fluctuate with small oscillations around zero in the bulk regions. As a consequence, the local contribution to the interfacial tension is located only at the interfaces, with an increase in the stress in the O/W interface region. Therefore, the accuracy of the interfacial tension calculation is achieved for all ϕ values, and curvature effects are not detected as Eq. (9) is only valid for flat interfaces.⁴⁴ As it can be seen, both pick heights and interface region width

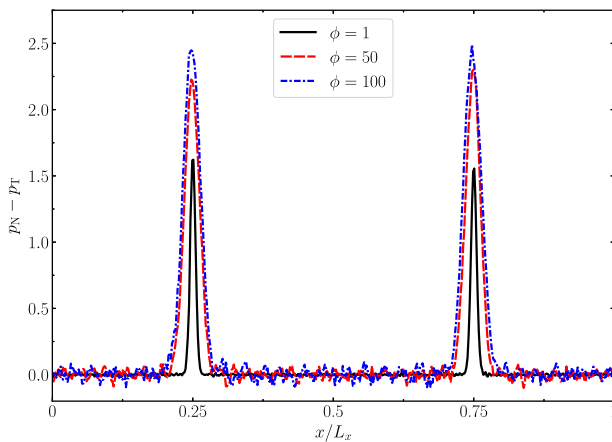


FIG. 4. Stress profiles (difference between normal and tangential pressures, $p_N - p_T$) along the normalized x -direction normal to the interfaces at increasing coarse-graining ratios ϕ for the simple DPD O/W system with $a_{WO} = 50$.

increase as the coarse-graining ratio ϕ increases, determining an increment in the IFT' value [see Eq. (9)]. This can be referred to as the combined effect of scaling both $r_{c,ij}$ and a_{ij} parameters according to Eq. (4).

Let us move now on the discussion of the ternary system made by oil, water, and surfactant (protein) when applying the scaling relations [Eq. (4)] to a reference system ($\phi = 1$) investigated in our previous work⁵ for two coarse-graining ratios ϕ . In order to study the equilibrium properties of such a system, the starting configuration of the DPD box consists of two symmetrical interfaces due to the periodic boundary conditions applied in the three directions. Figure 5 shows the equilibrated DPD boxes representing the oil–water planar interfaces covered by surfactant molecules for $\phi = 3008$ (case 3 in Table I) (a) and $\phi = 1504$ (b). Figure 6 reports the number density profiles of oil, water, and surfactant beads along the normalized x -direction for the coarse-graining ratios ϕ investigated in this work at two surfactant molecule number density c_p . By looking at Figs. 5 and 6, the symmetry of the equilibrated ternary system can be seen. Density profiles define the interfacial region that contains the surfactant layer and the bulk region that lies between the interfaces, highlighting the mutual interpenetration of each component at equilibrium. Therefore, the parameterization of the three species combined with the scaling procedure explained in Sec. II are able to maintain the structural properties of the interfacial system, even at a high level of coarse-graining ratio ϕ . In Fig. 6, it is straightforward to note that number density values are expressed as $\phi\rho'$ to make profiles comparable between ϕ equal to 3008 and 1504. Although the overall number density ρ is kept constant, the local bulk density of oil and water beads fluctuates around a value different from five due to the fact that the self-repulsion parameters used in this work for oil and water (a_{OO} and a_{WW} in Tables I and II) are not the same value.⁴⁸ A closer look at the surfactant density profiles reveals that an appreciable number of surfactant beads are not adsorbed at interfaces since the surfactant density values are not zero at the oil and water bulk regions. This effect is more relevant at higher c_p and for the case of $\phi = 3008$. In fact, at the same

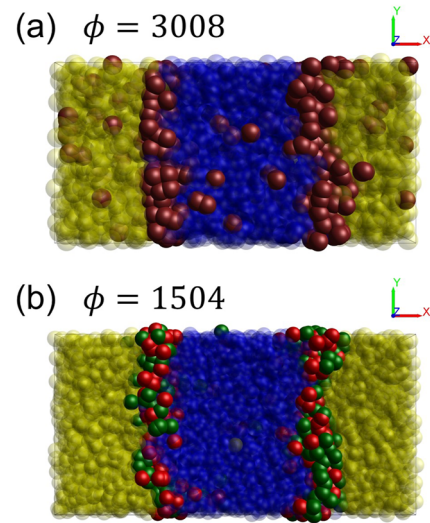


FIG. 5. Snapshots of equilibrated DPD boxes of the planar interfaces between oil (yellow) and water (blue) covered by surfactant molecules [brown beads for $\phi = 3008$ (case 3 in Table I) (a), green and red beads for $\phi = 1504$ (b)], at the surfactant molecule number density c_p equal to 3.05×10^{-4} (numbers per unit volume).

c_p , the surfactant density peaks are higher for $\phi = 1504$ than for $\phi = 3008$, meaning that a higher number of surfactant molecules are adsorbed at the interface in the former case than in the latter. This effect justifies the quantification of the surfactant molecules actually adsorbed at the interface by increasing surfactant concentration. This is obtained from the surfactant density profiles by implementing an automatic procedure to determine the protein surface density at equilibrium, as explained in the Appendix. However, Fig. 6 also shows that, when using the upscaled DPD model, a clear distinction between hydrophilic and hydrophobic parts in the surfactant molecule, as performed for $\phi = 1504$ (see Fig. 2 and Table II), provides better results in terms of preserving the reference conformation at equilibrium. In particular, for $\phi = 1504$, the surfactant molecules penetrate the water bulk to a much larger extent than the oil bulk, especially at higher c_p values, as already reported in our previous work.⁵

Figure 7 represents the most interesting result of this work. It reports the interfacial tension as a function of the surfactant (protein) surface number density by comparing the reference results for $\phi = 1$ from Ferrari *et al.*^{5,49} with those obtained in this work with $\phi = 3008$ (a) and $\phi = 1504$ (b). Three independent DPD runs were carried out, and the averaged values are shown together with the corresponding standard deviations. Error bars are generally smaller than symbols indicating the high reproducibility of the current DPD model. As it is shown that the interfacial tension scales following Eq. (10), it is expressed here as $\text{IFT}'/\phi^{1/3}$ in order to make its values comparable at different coarse-graining ratios ϕ . When no surfactant is added to the simulation box, it is important to highlight that, besides the scaling relation, the interfacial tension value between the oil and water phases is accurately reproduced by using the same parameterization of water and oil beads for different ϕ

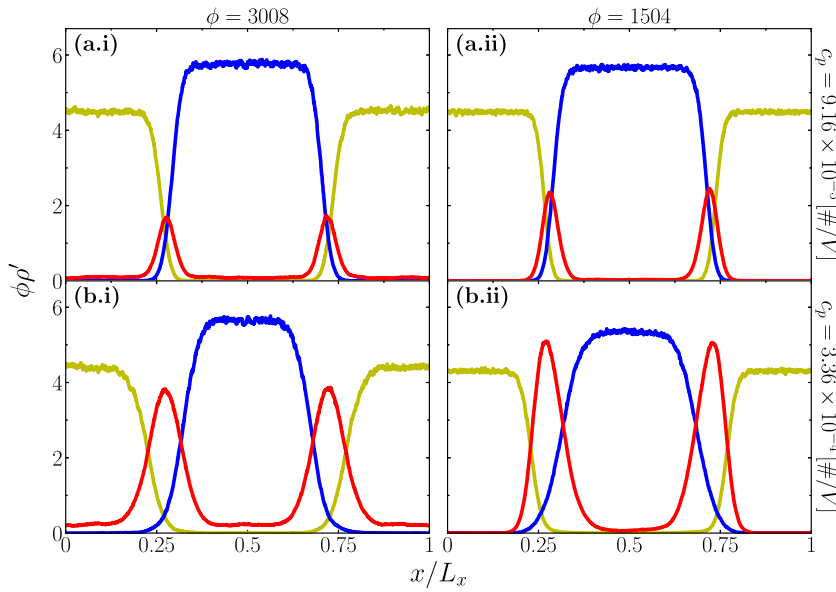


FIG. 6. Number density profiles of oil (yellow lines), water (blue lines), and surfactant (red lines) along the normalized x-direction normal to the interfaces with the coarse-graining ratio ϕ equal to 3008 (case 3 in Table I) [(a.i) and (b.i)] and 1504 [(a.ii) and (b.ii)] at two surfactant molecule number densities c_p [(a.i), (a.ii) and (b.i), (b.ii), respectively].

(Tables I and II). As it can be seen, a very good agreement is achieved for both ϕ values investigated here when increasing protein surface number density. Apart from a simple a parameter fine-tuning, it is possible to preserve the interfacial tension trend in an upscaled DPD

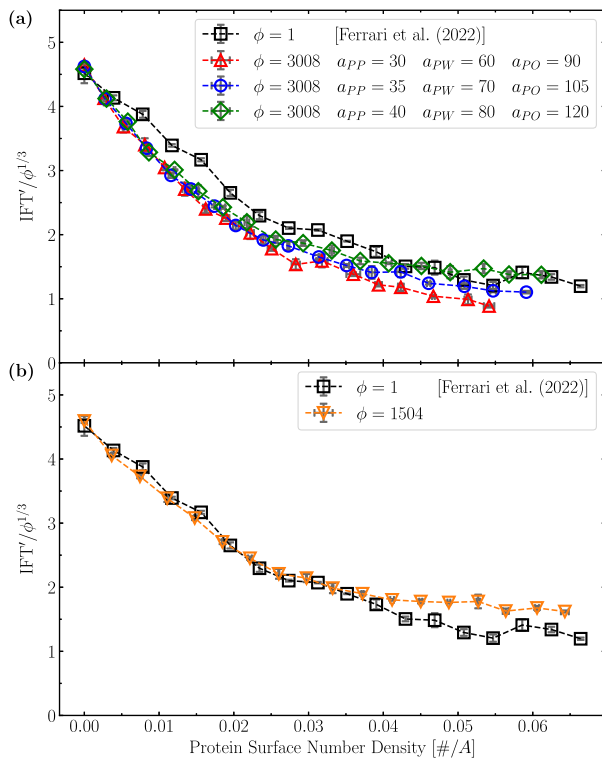


FIG. 7. Interfacial tension as a function of the protein surface number density, comparing between reference results for $\phi = 1$ and for $\phi = 3008$ (a) and $\phi = 1504$ (b). Error bars are estimated from three independent DPD simulations.

model with surfactant (protein) molecules. In both cases, the interfacial tension decreases as the protein surface density increases until it reaches a minimum value at the saturation of the interface. As it is shown, a further increase in protein surface concentration has almost no effect on the interfacial tension, which is a typical behavior of an interfacial system stabilized by surfactant proteins.^{50,51} However, some differences are identified with respect to the reference system with $\phi = 1$. With regard to $\phi = 3008$, all three protein bead parameterizations lead to larger deviations from the reference data at lower protein concentrations, while smaller ones correspond to the protein parameterization of case 3 in Table I at higher protein concentrations. On the other hand, concerning $\phi = 1504$, an almost perfect match with the reference case is obtained at lower protein concentrations. Nevertheless, the interfacial tension reaches its minimum value at the saturation of the interface at a lower protein concentration than that of $\phi = 1$. The values of protein surface number density are obtained as explained in the Appendix. As already illustrated in Fig. 6, each symbol corresponds to the same initial protein volume number density c_p in Fig. 7, thus the effect of the different number of molecules adsorbed at the interface depending on the coarse-graining ratio ϕ is here even more evident. In fact, when ϕ is equal to 3008, increasing the oil, water, and self-repulsion parameters of the P bead type (from case 1 to case 3 of Table I) leads to a better absorbing capability but a worse surfactant behavior in terms of the interfacial tension reduction. If the protein molecule is modeled as two bonded beads by distinguishing between the hydrophobic and hydrophilic contributions, as performed for $\phi = 1504$, the best adsorbing activity is obtained. In Fig. 8, the pressure trends for different ϕ values are then reported at increasing protein volume number density. When the oil/water interface is free of protein molecules, the pressure value increases non-linearly going from the case of $\phi = 1$ up to $\phi = 3008$ as expected by looking at Fig. 3(a). Then, clear differences in the pressure trends are observed. Although pressure decreases slightly linearly for $\phi = 1$ with increasing protein concentration, it increases non-linearly for $\phi = 3008$. This appears to be related

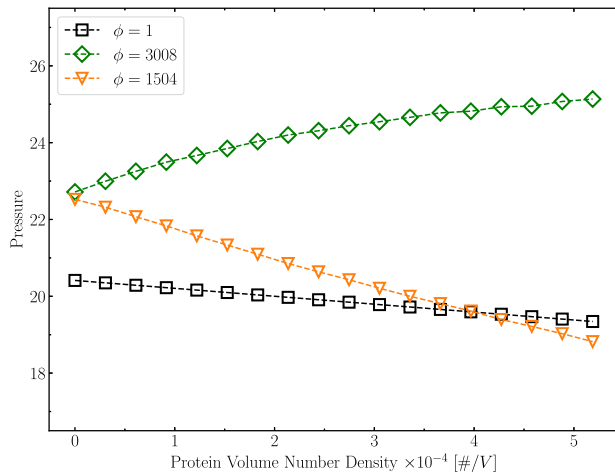


FIG. 8. Pressure trends for different ϕ values at increasing protein volume number density. Similar data are obtained with different parameterizations of the P bead type; thus, results for $\phi = 3008$ only referring to case 3 of Table I are reported. Error bars related to three independent DPD simulations are much smaller than the symbol size, thus they are not shown.

to the protein coarse-grained model used for $\phi = 3008$. In fact, if $\phi = 1504$ and the protein molecule is represented by at least two bead types, the pressure trend is decreasing as well. Nevertheless, its slope is relatively larger in absolute value than that of $\phi = 1$. Therefore, it seems that the pressure profile cannot be precisely

reproduced at higher coarse-graining levels when most molecular details are lost.

As the last result of this work, Fig. 9 shows an illustrative example of using the scaling procedure to simulate an oil droplet in bulk water in the presence of surfactants. As explained in Sec. III, the initial conditions and the physical space simulated are the same for $\phi = 3008$ and for $\phi = 1504$. Hence, similarities and differences between the two coarse-graining ratio cases are investigated. In both of them, it is important to highlight that the equilibrium configuration as a single droplet is observed due to the parameterization and the scaling procedure employed. This can demonstrate once again that the scaling relations in the DPD framework are able to describe different structural conformations. However, by comparing the $\phi = 3008$ case with the $\phi = 1504$ one, it is again shown that the adsorbing capability of protein molecules is better reproduced if they are modeled by two bonded beads than a single bead. This can be seen by looking at the time-frequency distributions of the radius of gyration value of the oil droplet covered by surfactant molecules and the corresponding snapshots of clipped simulation boxes in Fig. 9. In fact, the protein beads appear to be more dispersed in the simulation box for $\phi = 3008$ than for $\phi = 1504$, which is also represented by a bit smaller mean value of the droplet radius of gyration, meaning fewer protein molecules are adsorbed at the oil droplet interface with respect to the case of $\phi = 1504$. Moreover, the smaller standard deviation of the frequency distribution and the better quality of the fitting through the Gaussian distribution indicate more stability of the droplet modeled with $\phi = 1504$ than with $\phi = 3008$. If the same length conversion factor is used as in our previous work,⁵ then the corresponding mean

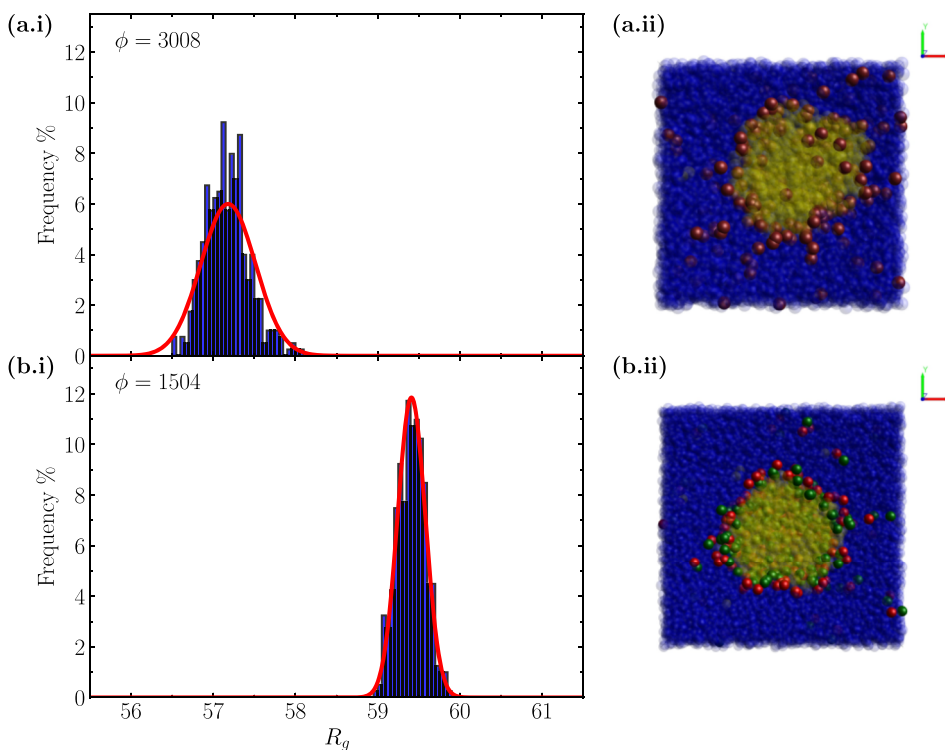


FIG. 9. Time-frequency distributions (blue histograms) of the radius of gyration value of an oil droplet covered by surfactant molecules in water bulk for $\phi = 3008$ (case 3 of Table I) (a.i) and for $\phi = 1504$ (b.i) and the relative Gaussian fitting curves (red lines). Corresponding snapshots of clipped simulation boxes are shown in (a.ii) and (b.ii), where oil and water are represented by yellow and blue beads, respectively, while protein molecules are represented by brown beads for $\phi = 3008$ and green and red beads for $\phi = 1504$.

values of the droplet radius of gyration are 43.7 and 45.4 nm for $\phi = 3008$ and for $\phi = 1504$, respectively. However, it must be stated that these numbers are based on speculative assumptions on spatial and time scales associated with DPD units. However, this seems in line with respect to previous studies on simulating a single droplet via DPD.^{52–54}

V. CONCLUSIONS

In this work, we explored the possibility of using classical DPD to describe an oil–water and an oil–water–surfactant system using the concept of level of coarse-graining, with the aim of obtaining a simplified model capable of reproducing properly the drop in interfacial tension observed with more detailed mesoscale simulations. We found that the classical DPD model is invariant with respect to the proper definition of the level of coarse-graining, as discussed in the work of Füchslin *et al.*³³ When dealing with interfacial systems, which are one of the most successful applications of the DPD method, they tend to exhibit a typical length scale due to the domain formation. This means that the independence of the length scale can no longer be achieved. However, in this work, we showed that, if an interfacial system can be simulated with DPD on a small scale, the scaling of interactions does not prevent a simulation on a larger scale unless specific issues are dealt with. Indeed, equilibrium properties of planar interfaces with and without a protein surfactant for different ratios of the level of coarse-graining were investigated by applying the scaling scheme. Although the level of description is much smaller, it was shown that the equilibrium interfacial tension trend can be conserved for different coarse-graining ratios besides a scaling factor. This can be achieved by a simple representation of the molecules involved, meaning that very few interaction parameters need to be set, thus decreasing the model complexity. The same approach for planar interfaces was also employed for a droplet configuration, showing that in both cases it is possible to maintain the domain conformation by applying an appropriate combined scaling procedure and coarse-graining parameterization. On the other hand, the pressure of interfacial systems appears to be not independent of the coarse-graining ratio, in contrast with the result of bulk fluids. The surface concentration of surfactants also seems to be related to the coarse-graining level and parameterization. Hence, possible applications of such findings will focus on investigating droplet coalescence and breakage events, which occur at a time- and space-scale larger than that of the thermal fluctuations of single particles. Future work will pave the way for a better understanding of to what extent DPD can be considered truly mesoscopic in terms of also dynamics properties by studying multi-component non-equilibrium systems.

ACKNOWLEDGMENTS

This work was carried out in the context of the VIMMP project (www.vimmp.eu), where the entire workflow will contribute to populate a marketplace for generic multiscale and multiphysics simulations. The VIMMP project has received funding from the European Union's Horizon 2020 Research Innovation Program under Grant Agreement No. 760907. We thank Jan-Willem Handgraaf (Siemens Industry Software Netherlands B.V., Galileiweg 8, 2333 BD, Leiden, The Netherlands) for providing us with the CULGI software employed in this work.

AUTHOR DECLARATIONS

Conflict of Interest

The authors have no conflicts to disclose.

Author Contributions

All authors contributed to the study conception and design. Software programming, data collection, and analysis were performed by Marco Ferrari. The first draft of the manuscript was written by Marco Ferrari, and all the authors iteratively corrected and contributed to the final version of the manuscript.

Marco Ferrari: Conceptualization (equal); Data curation (equal); Formal analysis (equal); Investigation (equal); Methodology (equal); Software (equal); Validation (equal); Visualization (equal); Writing – original draft (equal); Writing – review & editing (equal). **Gianluca Boccardo:** Conceptualization (equal); Project administration (equal); Resources (equal); Software (equal); Supervision (equal); Writing – review & editing (equal). **Daniele L. Marchisio:** Funding acquisition (equal); Project administration (equal); Resources (equal); Supervision (equal); Writing – review & editing (equal). **Antonio Buffo:** Conceptualization (equal); Formal analysis (equal); Methodology (equal); Resources (equal); Supervision (equal); Writing – review & editing (equal).

DATA AVAILABILITY

The data that support the findings of this study are openly available in Zenodo at <http://doi.org/10.5281/zenodo.6930825>, Ref. 55.

APPENDIX: CALCULATION OF THE SURFACE NUMBER DENSITY

The method used in this work to automatically determine the protein surface number density is here explained, as it has been seen that a certain number of surfactants are not adsorbed at the interface. This is similar to the procedure already employed to identify the bulk concentration of solutes in interfacial systems described in the literature.⁴⁸ Figure 10 shows an illustrative example of the method here used. From simulations of the ternary system with two symmetrical interfaces, the time-averaged number density profiles of protein molecules along the normalized x -direction normal to the interface expressed as $\phi\rho'$ are extracted (a) (see Figs. 5 and 6 for reference). The gradient of the number density is then computed with respect to x/L_x (b). The regions where the gradient fluctuates around zero define the bulk phases. The interface region can be identified by looking for spikes (positive and negative) in the gradient that are an order of magnitude greater than the fluctuations seen in the bulk regions. These spikes define the interface region to be included in number density calculations. Hence the standard deviation S_e of the gradient (the distance between horizontal gray dashed lines) is used to identify the distinction between bulk and interface regions. The first and last intersections between the gradient curve and horizontal lines in Fig. 10(b) define the interval limits ($\hat{x}_{1,a}$ and $\hat{x}_{1,b}$) of the interface region labeled as 1, where protein

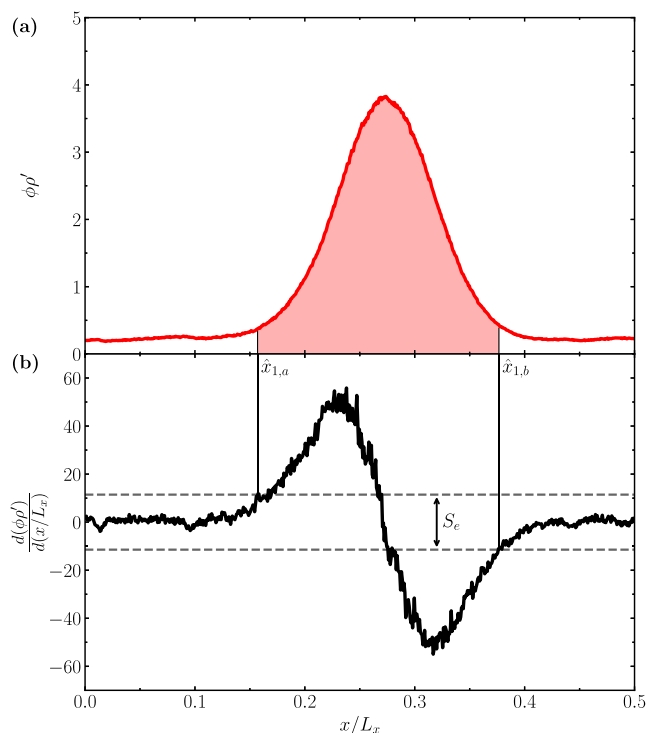


FIG. 10. Illustrative example on how the protein surface number density is determined in this work from the number density profile of surfactants along the normalized x -direction normal to the interface (a) by means of evaluating its gradient curve (b). The portion of the simulation box relative to the interface labeled as 1 is only shown. Further details on the meaning of the symbol notation can be found in the text.

molecules can be considered adsorbed at the interface. The same is performed for the interface labeled as 2 (not shown). From the area (in red) subtended by the number density profile, the equilibrated surface density of protein molecules at interface c_i is then obtained as follows:

$$c_i = \frac{L_x}{2n\phi L^2} \left(\int_{\hat{x}_{1,a}}^{\hat{x}_{1,b}} \phi p'(x/L_x) L^2 d(x/L_x) + \int_{\hat{x}_{2,a}}^{\hat{x}_{2,b}} \phi p'(x/L_x) L^2 d(x/L_x) \right), \quad (\text{A1})$$

where n corresponds to the number of beads representing the protein molecule, thus equal to 1 or 2 for $\phi = 3008$ or $\phi = 1504$, respectively (see Fig. 2). Hence, c_i values are used as abscissas in Fig. 7.

REFERENCES

- W. Norde, *Colloids and Interfaces in Life Sciences and Bionanotechnology* (CRC Press, Boca Raton, FL, 2011).
- C.-A. Palma, M. Cecchini, and P. Samori, "Predicting self-assembly: From empiricism to determinism," *Chem. Soc. Rev.* **41**, 3713–3730 (2012).
- A. J. Stone, *The Theory of Intermolecular Forces* (Oxford University Press, Oxford, UK, 2013).
- A. D. Lavino, M. Ferrari, A. A. Barresi, and D. Marchisio, "Effect of different good solvents in flash nano-precipitation via multi-scale population balance modeling-CFD coupling approach," *Chem. Eng. Sci.* **245**, 116833 (2021).
- M. Ferrari, J.-W. Handgraaf, G. Boccardo, A. Buffo, M. Vanni, and D. L. Marchisio, "Molecular modeling of the interface of an egg yolk protein-based emulsion," *Phys. Fluids* **34**, 021903 (2022).
- P. J. Hoogerbrugge and J. M. V. A. Koelman, "Simulating microscopic hydrodynamic phenomena with dissipative particle dynamics," *Europhys. Lett.* **19**, 155–160 (1992).
- P. Español and P. Warren, "Statistical mechanics of dissipative particle dynamics," *Europhys. Lett.* **30**, 191–196 (1995).
- R. D. Groot and P. B. Warren, "Dissipative particle dynamics: Bridging the gap between atomistic and mesoscopic simulation," *J. Chem. Phys.* **107**, 4423–4435 (1997).
- W. Pan, B. Caswell, and G. E. Karniadakis, "Rheology, microstructure and migration in Brownian colloidal suspensions," *Langmuir* **26**, 133–142 (2010).
- A. Panchenko, D. F. Hinz, and E. Fried, "Spatial averaging of a dissipative particle dynamics model for active suspensions," *Phys. Fluids* **30**, 033301 (2018).
- Q. Nie, Y. Zhong, and H. Fang, "Study of a nanodroplet breakup through many-body dissipative particle dynamics," *Phys. Fluids* **31**, 042007 (2019).
- Z. Li, G.-H. Hu, Z.-L. Wang, Y.-B. Ma, and Z.-W. Zhou, "Three dimensional flow structures in a moving droplet on substrate: A dissipative particle dynamics study," *Phys. Fluids* **25**, 072103 (2013).
- Y. Kong, C. W. Manke, W. G. Madden, and A. G. Schlijper, "Effect of solvent quality on the conformation and relaxation of polymers via dissipative particle dynamics," *J. Chem. Phys.* **107**, 592–602 (1997).
- H. Drogheiti, I. Pagonabarraga, P. Carbone, P. Asinari, and D. Marchisio, "Dissipative particle dynamics simulations of tri-block co-polymer and water: Phase diagram validation and microstructure identification," *J. Chem. Phys.* **149**, 184903 (2018).
- A. Maiti and S. McGrother, "Bead-bead interaction parameters in dissipative particle dynamics: Relation to bead-size, solubility parameter, and surface tension," *J. Chem. Phys.* **120**, 1594–1601 (2004).
- A. Khedr and A. Striolo, "DPD parameters estimation for simultaneously simulating water-oil interfaces and aqueous nonionic surfactants," *J. Chem. Theory Comput.* **14**, 6460–6471 (2018).
- A. Ghoufi, P. Malfreyt, and D. J. Tildesley, "Computer modelling of the surface tension of the gas-liquid and liquid-liquid interface," *Chem. Soc. Rev.* **45**, 1387–1409 (2016).
- M. Ndao, F. Goujon, A. Ghoufi, and P. Malfreyt, "Coarse-grained modeling of the oil-water-surfactant interface through the local definition of the pressure tensor and interfacial tension," *Theor. Chem. Acc.* **136**, 21 (2017).
- X. Wang, K. P. Santo, and A. V. Neimark, "Modeling gas-liquid interfaces by dissipative particle dynamics: Adsorption and surface tension of cetyl trimethyl ammonium bromide at the air-water interface," *Langmuir* **36**, 14686–14698 (2020).
- V. Y. Hon, I. M. Saaid, I. C. H. Chai, N. A. A. M. Fauzi, E. Deguillard, J. van Male, and J.-W. Handgraaf, "Microemulsion interface model for chemical enhanced oil recovery design," *J. Pet. Sci. Eng.* **212**, 110279 (2022).
- S. R. Euston, "14 - Modelling and computer simulation of food structures," in *Food Microstructures, Woodhead Publishing Series in Food Science, Technology and Nutrition*, edited by V. Morris and K. Groves (Woodhead Publishing, 2013), pp. 336–385.
- S.-I. Lin, M.-y. Xu, and Z.-r. Yang, "Dissipative particle dynamics study on the mesostructures of n -octadecane/water emulsion with alternating styrene-maleic acid copolymers as emulsifier," *Soft Matter* **8**, 375–384 (2012).
- F. Alvarez, E. A. Flores, L. V. Castro, J. G. Hernández, A. López, and F. Vázquez, "Dissipative particle dynamics (DPD) study of crude oil-water emulsions in the presence of a functionalized Co-polymer," *Energy Fuels* **25**, 562–567 (2011).
- L. Rekvig, B. Hafskjold, and B. Smit, "Molecular simulations of surface forces and film rupture in oil/water/surfactant systems," *Langmuir* **20**, 11583–11593 (2004).
- F. Goujon, A. Dequidt, A. Ghoufi, and P. Malfreyt, "How does the surface tension depend on the surface area with coarse-grained models?" *J. Chem. Theory Comput.* **14**, 2644–2651 (2018).

- ²⁶N. Lauriello, J. Kondracki, A. Buffo, G. Boccardo, M. Bouaifi, M. Lisal, and D. Marchisio, "Simulation of high Schmidt number fluids with dissipative particle dynamics: Parameter identification and robust viscosity evaluation," *Phys. Fluids* **33**, 073106 (2021).
- ²⁷P. Español and P. B. Warren, "Perspective: Dissipative particle dynamics," *J. Chem. Phys.* **146**, 150901 (2017).
- ²⁸M. Ellero and P. Español, "Everything you always wanted to know about SDPD* (*but were afraid to ask)," *Appl. Math. Mech.* **39**, 103–124 (2018).
- ²⁹A. Vázquez-Quesada, M. Ellero, and P. Español, "Consistent scaling of thermal fluctuations in smoothed dissipative particle dynamics," *J. Chem. Phys.* **130**, 034901 (2009).
- ³⁰J. Zhao, S. Chen, K. Zhang, and Y. Liu, "A review of many-body dissipative particle dynamics (MDPD): Theoretical models and its applications," *Phys. Fluids* **33**, 112002 (2021).
- ³¹Z. Li, Y.-H. Tang, H. Lei, B. Caswell, and G. E. Karniadakis, "Energy-conserving dissipative particle dynamics with temperature-dependent properties," *J. Comput. Phys.* **265**, 113–127 (2014).
- ³²P. Español, "Fluid particle model," *Phys. Rev. E* **57**, 2930–2948 (1998).
- ³³R. M. Füchslin, H. Fellermann, A. Eriksson, and H.-J. Ziock, "Coarse graining and scaling in dissipative particle dynamics," *J. Chem. Phys.* **130**, 214102 (2009).
- ³⁴M. Arienti, W. Pan, X. Li, and G. Karniadakis, "Many-body dissipative particle dynamics simulation of liquid/vapor and liquid/solid interactions," *J. Chem. Phys.* **134**, 204114 (2011).
- ³⁵N. Mai-Duy, N. Phan-Thien, T. Y. N. Nguyen, and T. Tran-Cong, "Coarse-graining, compressibility, and thermal fluctuation scaling in dissipative particle dynamics employed with pre-determined input parameters," *Phys. Fluids* **32**, 053313 (2020).
- ³⁶J. A. Backer, C. P. Lowe, H. C. J. Hoefsloot, and P. D. Iedema, "Combined length scales in dissipative particle dynamics," *J. Chem. Phys.* **123**, 114905 (2005).
- ³⁷J. R. Spaeth, T. Dale, I. G. Kevrekidis, and A. Z. Panagiotopoulos, "Coarse-graining of chain models in dissipative particle dynamics simulations," *Ind. Eng. Chem. Res.* **50**, 69–77 (2011).
- ³⁸E. Moeendarbary, T. Y. Ng, and M. Zangeneh, "Dissipative particle dynamics: Introduction, methodology and complex fluid applications—A review," *Int. J. Appl. Mech.* **01**, 737–763 (2009).
- ³⁹F. Sepehr and S. J. Paddison, "Dissipative Particle Dynamics interaction parameters from *ab initio* calculations," *Chem. Phys. Lett.* **645**, 20–26 (2016).
- ⁴⁰L. Verlet, "Computer "Experiments" on classical fluids. I. Thermodynamical properties of Lennard-Jones molecules," *Phys. Rev.* **159**, 98–103 (1967).
- ⁴¹P. M. Pieczywek, W. Płaziński, and A. Zdunek, "Dissipative particle dynamics model of homogalacturonan based on molecular dynamics simulations," *Sci. Rep.* **10**, 14691 (2020).
- ⁴²K. P. Santo and A. V. Neimark, "Dissipative particle dynamics simulations in colloid and interface science: A review," *Adv. Colloid Interface Sci.* **298**, 102545 (2021).
- ⁴³R. D. Groot and K. L. Rabone, "Mesoscopic simulation of cell membrane damage, morphology change and rupture by nonionic surfactants," *Biophys. J.* **81**, 725–736 (2001).
- ⁴⁴J. H. Irving and J. G. Kirkwood, "The statistical mechanical theory of transport processes. IV. The equations of hydrodynamics," *J. Chem. Phys.* **18**, 817–829 (1950).
- ⁴⁵J. G. E. M. Fraaije, J. van Male, P. Becherer, and R. Serral Gracià, "Coarse-grained models for automated fragmentation and parametrization of molecular databases," *J. Chem. Inf. Model.* **56**, 2361–2377 (2016).
- ⁴⁶Culgi B. V., The Netherlands, The Chemistry Unified Language Interface (CULGI), www.culgi.com, version 13.0.0 (2020).
- ⁴⁷P. Vanya, J. Sharman, and J. A. Elliott, "Invariance of experimental observables with respect to coarse-graining in standard and many-body dissipative particle dynamics," *J. Chem. Phys.* **150**, 064101 (2019).
- ⁴⁸R. L. Anderson, D. J. Bray, A. S. Ferrante, M. G. Noro, I. P. Stott, and P. B. Warren, "Dissipative particle dynamics: Systematic parametrization using water-octanol partition coefficients," *J. Chem. Phys.* **147**, 094503 (2017).
- ⁴⁹M. Ferrari, J.-W. Handgraaf, G. Boccardo, A. Buffo, M. Vanni, and D. L. Marchisio (2021). "Dataset for "Molecular modeling of the interface of an egg yolk protein-based emulsion," Zenodo, Dataset <https://doi.org/10.5281/zenodo.5703247>
- ⁵⁰D. E. Graham and M. C. Phillips, "Proteins at liquid interfaces: II. Adsorption isotherms," *J. Colloid Interface Sci.* **70**, 415–426 (1979).
- ⁵¹V. B. Fainerman, E. H. Lucassen-Reynders, and R. Miller, "Description of the adsorption behaviour of proteins at water/fluid interfaces in the framework of a two-dimensional solution model," *Adv. Colloid Interface Sci.* **106**, 237–259 (2003).
- ⁵²D. Pan, N. Phan-Thien, and B. C. Khoo, "Dissipative particle dynamics simulation of droplet suspension in shear flow at low Capillary number," *J. Non-Newtonian Fluid Mech.* **212**, 63–72 (2014).
- ⁵³S. Chen, N. Phan-Thien, X.-J. Fan, and B. C. Khoo, "Dissipative particle dynamics simulation of polymer drops in a periodic shear flow," *J. Non-Newtonian Fluid Mech.* **118**, 65–81 (2004).
- ⁵⁴Y. Zhang, J. Xu, and X. He, "Effect of surfactants on the deformation of single droplet in shear flow studied by dissipative particle dynamics," *Mol. Phys.* **116**, 1851–1861 (2018).
- ⁵⁵M. Ferrari, G. Boccardo, D. L. Marchisio, and A. Buffo (2022). "Dataset for "Application of dissipative particle dynamics to interfacial systems: Parameterization and scaling," Zenodo, Dataset <https://doi.org/10.5281/zenodo.6930825>